What do arc magmatism trace element patterns and Sr-Nd-Pb isotopic data reflect: Insights from the Urumieh-Dokhtar magmatic arc of Iran

Mohammad Reza Ghorbani[1], Meysam Akbari[1,2], Ian T. Graham[3], Mathieu Benoit[4], Fatemeh Sepidbar[5]

[1] Department of Geology, Tarbiat Modares University (TMU), Tehran, 14115-175, Iran
[2] Research Institute for Earth Sciences, Tehran, 13185-14194, Iran
[3] Earth and Sustainability Science Research Centre, School of Biological, Earth and Environmental Sciences, The University of New South Wales, Sydney, NSW 2052, Australia
[4] Géosciences Environnement Toulouse (GET), Observatoire Midi Pyrénées, Université de Toulouse, CNRS, IRD, 14 Avenue E. Belin, Toulouse, F-31400 France
[5] Department of Geology, Faculty of Science, Ferdowsi University of Mashhad, Mashhad, Iran

Correspondence to: Mohammad Reza Ghorbani (ghorbani@modares.ac.ir)

Abstract. Mafic volcanic rocks from the Cenozoic Urumieh-Dokhtar Magmatic Arc (UDMA) of Iran, a segment of the Alpine-Himalayan orogenic belt, provide rather restricted ranges of trace element abundances and patterns and Sr-Nd-Pb isotopic signatures. However, they are distinct enough to help characterize the geochemical signatures inherited from their arc system components. The volcanic rocks are classified into three series; the LILE-rich, LILE-poor, and incompatible trace elements-rich series (ITE-rich series; which includes samples with OIB-like patterns). The LILE-rich series is derived from a mantle source metasomatized by fluid-rich-slab partial melts whereas the LILE-poor series, high in immobile and highly incompatible elements that include La and Ce, is derived from a mantle source metasomatized by fluid-poor-slab partial melts. Slab melting is favoured by the young, hot slab subduction of a then narrow, contracting Neotethyan oceanic plate. The ITE-rich series bear the signatures of mantle metasomatized by slab partial melts that was induced by and reacted with asthenospheric mantle that ascended through a slab window or rupture. Given almost primitive geochemical signatures of the mafic rocks, the Sr-Nd isotopic modelling indicates a mantle wedge:slab melt:sediment melt contribution of 45:27.5:27.5 and 55:09:36 for the LILE-rich and LILE-poor series respectively. The mafic volcanic rocks which extend from the mantle array (i.e., NHRL) towards an enriched mantle on the Pb-Pb isotopic plots further support this finding. Eocene to Early Miocene ages for these three series favour intermittent volcanism of the three rock series over an extended period of time rather than single episodic magmatism for each geochemically distinct magma series. Dominance of the LILE-rich series rocks in the northern part of the study area (the Kahak area), points to a more hydrous, more altered slab as compared to the central part of the study area where the LILE-poor series is dominant.

1 Introduction

The origin and evolution of subduction-related or arc affinity volcanic rocks have been the subject of scrutiny for many years (Cross and Pilger, 1982; Hildreth and Moorbath, 1988; Benoit et al., 2002; Bouilhol et al., 2013; van Hinsbergen et al., 2020), and those from the Cenozoic Urumieh-Dokhtar Magmatic Arc (UDMA) of Iran are no exception (Berberian and King, 1981; Agard et al., 2005; Chiu et al., 2013; Ghorbani et al., 2014). However, no major review has been undertaken to present an overview of the compositional spectrum and primitive end-members for the magmatic, mainly volcanic rocks from the UDMA. Involvement of a number of distinct source components, such as mantle, fluids, or partial melts derived from the subducting slab and overlying sediments, leads to a wide variation in chemistry, particularly trace element abundances and patterns of the subduction-related volcanic rocks (Pearce et al., 1990; Ewart et al., 1998; Xia, 2014). Revealing the source components of volcanic rocks is amongst the most important but also most difficult tasks in the study of magmatic arcs. Moreover, the source components are usually obscured by secondary or differentiation processes. This is especially the case for active continental margins, where the overlying thick crustal rocks may undergo partial melting to further contribute to the magmatism (Spikings et al., 2015; Di Giuseppe et al., 2021). Focusing on the 'most mafic' volcanic rocks, represented by the samples in the 48 to 57 wt% silica range, is a reliable approach in order to avoid the secondary processes that blur the pristine magmatic components.

Based on the major, trace element and Sr-Nd-Pb isotopic data of a collection of mafic volcanic rocks sampled from multiple areas across the central part of the UDMA (Fig. 1), this study tries to infer some key implications as to the nature of the geodynamic evolution as well as mantle and crustal source regions that melted and /or dehydrated to produce them. In order to achieve this goal, 1- abundances and patterns of incompatible trace elements and Sr-Nd-Pb isotopic ratios in the mafic volcanic rocks were investigated and three distinct series were found to occur and 2- considering the likely involvement of the mantle, slab fluids, slab melts and crustal components as well as the radiometric ages compiled from recent studies, a petrogenetic model is presented that sheds light on the geodynamic evolution of the three rock series.

2 Geology of the study area

As a part of the Alpine-Himalayan Belt, the Zagros Orogeny stretches for nearly 2000 km from northwest to southern Iran. This orogeny is the consequence of subduction of the Neotethyan oceanic plate beneath central Iran and the final collision of the Arabia and Eurasia plates (Berberian and King, 1981; Alavi, 1994; Mohajjel and Fergusson, 2000). The Zagros Orogeny comprises three sections, the Zagros Fold and Thrust Belt (ZFTB), the Sanandaj-Sirjan Zone (SSZ), and the UDMA (Fig. 1.a). The UDMA, also known as the central Iran magmatic belt, and occurs as a thick mainly Eocene to Miocene volcanic succession of up to 3000 m thick that is intruded by plutonic bodies of mainly Oligocene to Miocene ages. An 'active continental margin' model (Berberian and Berberian 1981; Moinevaziri 1985) for the subduction predominates, though a few studies report some similarities to 'island arc' magmatism (Ghorbani, 2006; Shahabpour, 2007).
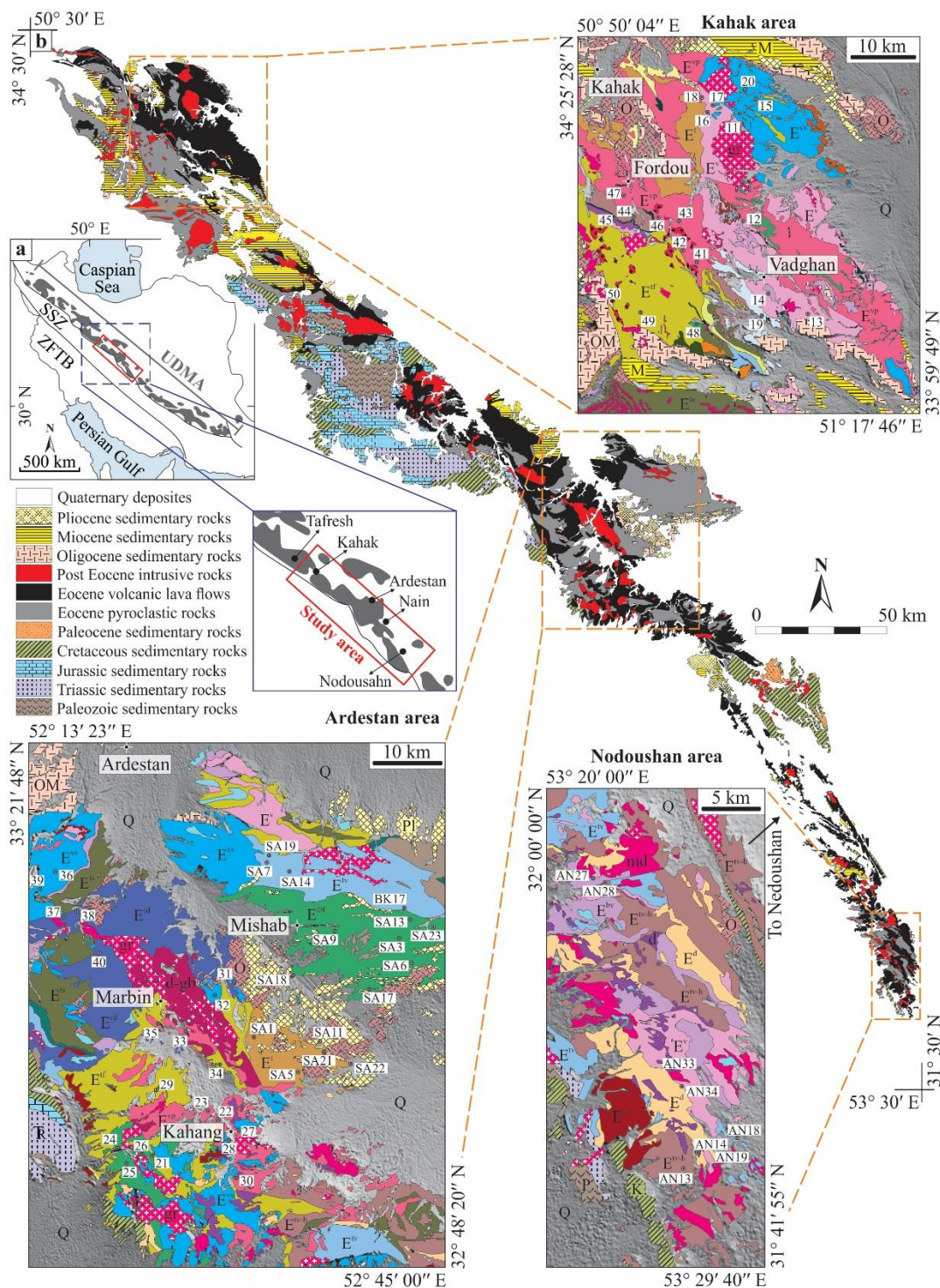
Figure 1: (a) Regional tectonomagmatic units of Iran (after Alavi, 1994). The gray fields show the Urumieh-Dokhtar magmatic arc (UDMA). Abbreviations: SSZ, Sanandaj-Sirjan Zone; ZFTB, Zagros Fold and Thrust Belt. (b) Simplified geological map of the

central UDMA compiled based on the geological maps on a scale of 1:100.000 for Kahak (Ghalamghash et al., 1988), Kashan (Radfar and Alaie-Mahabadi, 1993), Natanz (Khalatbari Jafari and Alaie-Mahabadi, 1995), Tarq (Zahedi and Rahmati, 2002), Ardestan (Radfar and Amini Chehragh, 1999), Shahrab (Bahroudi and Fonoudi, 1997), Kuhpayeh (Radfar et al., 2002), Kajan (Amini and Amini Chehragh, 2003), Nain (Alaie-Mahabadi and Foudazi, 2004), Sarve-Bala (Amidi et al., 1989), and Kafeh-Taghestan (Ghalamghash et al., 2005). More detailed geological maps are provided for three segments of the central UDMA. Location of the samples selected for geochemical analyses are also shown. For legend and lithostratigraphic columns of these three segments of the central UDMA see Fig. S1.

Based on interbedded fossiliferous beds, the UDMA volcanic succession has been traditionally attributed to the Eocene (e.g., Berberian and King, 1981; Emami et al., 1993), and is divided into six units, E_1-E_6, on the geological maps drafted by the Geological Survey of Iran (cf. for lithostratigraphic columns of different segments of the study area see Fig. S1). Verdel et al. (2011), based on the dominantly Eocene ages obtained for the volcanic rocks from the Tafresh area (i.e., the northernmost part of the central UDMA), introduced the Eocene flare-up model as being responsible for the Cenozoic magmatism of the UDMA whereby extension induced partial melting of the metasomatized mantle, producing the Eocene calc-alkaline volcanic rocks. This model suggests that the gradual slab rollback caused asthenospheric upwelling and triggered the Oligocene OIB affinity volcanic rocks.

Multiple age dating of the volcanic rocks from the UDMA prompted Chiu et al. (2013) to infer that magmatic flare-up was not limited to the Eocene but also extended into the Oligocene. Further age dating by Ghorbani et al. (2014) extended the widespread magmatic activity in the UDMA even further into the Miocene. Having presented the age-dated samples from the central UDMA on a generalized stratigraphic column that was compiled based on the geological maps, Ghorbani et al. (2014) implied a discrepancy. The discrepancy in ages (i.e., the difference between the real age and the presumed Eocene age), indicates the necessity for a revision of the E_1-E_6 divisions. An improvement in the stratigraphic column of the UDMA has recently begun to emerge (see Fig. 2 in: Sepidbar et al., 2021); that is the Oligocene-Miocene magmatic records grow at the expense of Eocene magmatic records. Moradi et al. (2021) also reported Miocene ages for the volcanic rocks from the Neragh area of the central part of the UDMA. Adakitic rocks have also been reported from the central UDMA (Omrani et al., 2008; Ghorbani and Bezenjani, 2011; Ghorbani et al., 2014; Ahmadian et al., 2016); these however postdate the Middle Miocene and have been attributed to high-pressure slab melting.

The present literature on the evaluation of the compositional aspects of the magmatic rocks from the UDMA is limited. Volcanic rocks with negative Nb-Ta anomalies are attributed to subduction (Pearce, 1982; Kelemen et al. 2005) whereas some rocks with higher Nb-Ta abundances have been regarded as being derived from an asthenospheric mantle source (Verdel et al., 2011; Yeganehfar et al., 2013). A few studies on the UDMA include Sr-Nd-Pb isotopic data on the mafic volcanic rocks (Yeganehfar et al., 2013; Jolani Varzeghani, 2017; Khodami, 2019; Sepidbar et al., 2019; Moradi et al., 2021); these works collectively attribute the volcanic rocks to the mixing of varying, marginal proportions of crustal melts with dominating mantle-derived partial melts in a subduction setting.

The UDMA is mainly dominated by intermediate to felsic volcanic and pyroclastic rocks. These include andesites-
100   trachyandesites, dacites-rhyolites, and tuffs-tuff breccia-ignimbrites respectively. Mafic volcanic rocks occur sporadically and
include basalts, alkali basalts, and trachybasalts. The apparent scarcity of mafic rocks in the UDMA volcanic successions has
been a major obstacle in the evaluation of end-members of the source regions and materials that evolved to generate the
volcanic successions. The paucity of mafic rocks makes it difficult to follow the melt compositional evolution or liquid line of
descent (Wilson, 1989). To overcome this paucity of mafic rocks, the current study carried out widespread sampling from
105   multiple areas across the central part of the UDMA (Fig. 1). This furnished a representative set of the mafic-intermediate
volcanic rocks for detailed petrological and geochemical investigations.

The volcanic rocks sampled in this study are lavas ranging in thickness from meters to tens of meters. Porphyritic to aphyric
textures of the volcanic rocks confirm their eruptive nature. A simplified geological map of the UDMA is shown in Fig.1,
which is compiled based on the present geological maps (see caption in Fig. 1 for details). The present study area comprises
110   three segments from northwest to southeast; these are Kahak (including Fordou and Vadghan), Ardestan (including Mishab,
Marbin, and Kahang), and Nodoushan, respectively (Fig. 1.b). Integrating these volcanic segments into a larger tectonic context
will be a worthwhile endeavour as a roadmap for future studies.

3 Petrographic analysis

Petrography was focused on samples of the volcanic series considered representative of the present study areas from the
115   UDMA (Fig. 1.b). The basaltic rocks of the present study mostly contain sparse clinopyroxene along with minor plagioclase
phenocrysts in a fine-grained groundmass. The mafic–intermediate volcanic rocks are slightly to moderately porphyritic in
texture (Fig. S2). While the groundmass in some samples is almost aphyric, other samples show a cryptocrystalline to
microcrystalline groundmass composed of glass, plagioclase, clinopyroxene, and Fe-Ti oxides.

Textural and mineralogical characteristics of the mafic volcanic rocks from the study area are briefly presented in Table 1.
120   Although glass constitutes the major component of the groundmass, most samples include variable quantities of fine-grained
feldspars, clinopyroxenes, and Fe-Ti oxides. Olivine and orthopyroxene phenocrysts are rare, mostly altered, and found as
pseudomorphed grains (i.e., replaced by chlorite and other secondary minerals). Glomeroporphyritic textures are found in a
few samples and mainly include clinopyroxene and plagioclase. Amphibole was only found in two samples from the
Nodoushan area where the mafic volcanic rocks are rare and limited to andesitic rocks (see below). Only fresh samples were
125   selected, so secondary minerals such as sericite, chlorite, calcite, and epidote which are the alteration products of silicate
minerals are rare if present at all. However, before using the geochemical data, the possibility of alteration and its effect on
element mobility are discussed below (see Section 6.1).

130 **Table 1: Modal mineralogy of LILE-rich, LILE-poor, and ITE-rich series. Petrographic features of the individual samples are provided in Table S1. Photomicrographs of samples with bold numbers are provided in Fig S2. The abbreviations Fld, Pl, Cpx, Opx, Ol, Amp, and Opq stand for feldspar, plagioclase, clinopyroxene, orthopyroxene, olivine, amphibole, and opaque minerals respectively.**

Rock series	Sample No.	Texture	Groundmass	Phenocrysts (vol%)
LILE-poor	**UC30**, UD32, UD37	Vitrophyric	Glass ± Fld ± Cpx ± Opq	≤ 5, Ol ± Pl ± Cpx
	UC22, UC25, UC26 **UC27**, **UC28**, UD33, UD36, UD38, SA1, SA9	Porphyritic	Cryptocrystalline to Microcrystalline Glass + Fld + Opq ± Cpx	≤ 5, Pl ± Ol ± Opx ± Cpx ± Opx
	UC23, UC24, UD34, **UD35**, UD39	Porphyritic	Cryptocrystalline to Microcrystalline Glass + Fld + Cpx + Opx	< 10, Pl ± Cpx ± Ol ± Opx ± Opq
	UC21, UD31	Porphyritic	Cryptocrystalline Glass + Fld ± Cpx ± Opx	< 20, Pl ± Ol ± Cpx
	SA13, SA23	Microgranular Fld + Opq ± Ol ± Opx	± Glass	
LILE-rich	AN14, AN18, AN33 UE41	Vitrophyric	Glass ± Fld ± Opq	≤ 5, Pl ± Cpx ± Opx ± Opq
	UB13, UB14, UE42	Porphyritic	Microcrystalline to Cryptocrystalline Fld ± Glass ± Cpx ± Opx	≤ 5, Pl ± Cpx
	UB12, UB15, **UB16**, **UB18**, UB19, UB20, SA7, **SA18**, AN34, UE45, UE47, **UE48**, UE50	Porphyritic	Cryptocrystalline Glass + Fld ± Cpx ± Opx	< 15, Pl ± Cpx ± Ol ± Opx ± Amp
	UB17, SA19, UE44	Porphyritic	Glass + Fld ± Cpx ± Opq	< 25, Pl ± Opx ± Opq
	AN13	Porphyritic	Glass	< 10, Pl + Amp + Cpx + Opx
	AN27	Microgranular Pl + Cpx + Amp + Opq		
	UE43, UE49	Microgranular (Pl + Cpx + Opx)		
ITE-rich	**SA14**, SA17	Vitrophyric	Cryptocrystalline Glass ± Fld ± Opq	≤ 5, Pl
	UE46, **SA21**	Porphyritic	Cryptocrystalline to Microcrystalline Glass + Fld + Cpx + Opq	≤ 5, ± Pl ± Ol
	UB11, SA3, **SA11**	Porphyritic	Cryptocrystalline Glass + Fld ± Cpx ± Opq	< 15, Pl ± Cpx ± Ol ± Opx ± Opq
	SA6	Microgranular Fld + Opq		

4 Methods

135 A representative set of 66 mafic–intermediate volcanic rocks from the study area was analyzed for major and trace elements (Table S2). After a detailed examination of the major and trace element geochemistry of the rocks, 14 samples were selected for Sr-Nd-Pb isotopic analyses (Table S3). In order to avoid altered samples, the representative set was selected based on detailed petrographic examination of 250 thin sections across the region.

4.1 Major and trace element analysis

140 Whole-rock analyses for major elements were obtained by X-ray fluorescence (XRF) at the Mark Wainright Analytical Centre, University of New South Wales, Sydney, Australia, following the procedures of Norrish and Hutton (1969). The analyses were carried out on a Phillips PW2400 XRF spectrometer using 40-mm glass disks. Inductively coupled plasma–mass spectrometry (ICP-MS) was used for rare earth and trace elements analyses of the whole-rock samples at the Genalysis Laboratory, Perth, Australia, using the Perkin–Elmer ICP-MS 9000 (i.e., 51 samples marked by numbers in normal fonts in Table S2) and the

145 School of Geography, Earth and Atmospheric Sciences, University of Melbourne, Victoria, Australia using the NexION 2000 (i.e., for 15 samples marked by numbers in italic fonts in Table S2).

Some accessory minerals are trace element repositories that resist the mixed acid digest method. To ensure complete digestion while maintaining good sensitivity, a combination digestion method (i.e., a mixed acid digest and multi-fusion) was used. The details are as follows. The pulp was digested in $HNO_3/HClO_4$ on a hot plate and then cooled. HF was added and digestion

150 continued on the hotplate; the mixture was then cooled and salts were leached with an HCl/HNO_3 mix on the hotplate. The solution was then cooled and filtered to recover undigested material fused with minimal Li metaborate–tetraborate flux. The melt was produced and then leached with HCl. Leach solutions were combined for the ICP-MS analysis.

Both in-house and internationally certified standards were analyzed (Table S4) and gave an overall relative procedural error of better than 3%. Analytical reproducibility was also examined. For the rare earth and trace elements, errors were evaluated

155 to be better than 3% except for Nb, Ta, and U (8%). Duplicate analyses indicate that the errors for major elements are better than 1% except for alkaline elements (5%). The whole-rock analysis totals are in the range from 98.79 to 101.83 wt% with a mean of 100.80 wt% (Table S2). The diagrams depicted are based on the major element analyses recalculated to 100 wt%, on an anhydrous basis.

4.2 Sr-Nd-Pb isotopic analysis

160 The isotopic data was obtained from GET-OMP, Toulouse University (France), using the Thermo Scientific TRITON+ solid source mass spectrometer, following the procedures outlined in Li et al. (2011, 2012). Before measurement, about 100 mg of whole rock powder was weighed in a teflon beaker and dissolved in a mixture HF/HNO_3 1:1. After dissolution, samples were diluted in 1 ml 2% HNO_3 and Nd/Sr were extracted from the matrix (2N HNO_3) using a combination of Sr-Spec and Thru-spec Eichrom resins. Mixed Sr and REE were loaded on a Re filament and were run sequentially (first Sr then Nd) using a

165 double Re filament protocol. Monitoring of the interferences of ^{87}Rb and ^{144}Sm were proceeded according to the protocol of Li et al. (2012) and the quality and reproducibility of the measurements were controlled using a sequential measurement of isotopic standards (SRM 987 and JNdi), doped isotopic standards (NBS 987+ Rb and JNdi + Sm) and laboratory-dedicated Sr+REE artificial solutions. Standard reproducibilities are ^{87}Sr/^{86}Sr = 0.710280 ± 15 for SRM-987 and 0.512100 ± 10 for JNdi (pure and doped) and fall within the recommended values. Measured blanks are 25 pg for Nd and 325 pg for Sr. ^{87}Sr/^{86}Sr and

170 ^{143}Nd/^{144}Nd ratios were normalized against ^{86}Sr/^{88}Sr = 0.1194 and ^{146}Nd/^{144}Nd = 0.7219 respectively, after corrections from isobaric interferences using ^{87}Rb/^{85}Sr = 0.387041 on ^{87}Sr and combination of ^{147}Sm/^{149}Sm=1.08583 and ^{147}Sm/^{144}Sm = 4.87090 on ^{144}Nd.

Pb fractions have been extracted from the matrix during the same elution protocol as Sr and Nd following the procedure of Pin and Gannoun (2017). Pb isotopes were determined on a Thermo Scientific TRITON+ solid source mass spectrometer using

175 the Rex Taylor Double Spike method. NBS 981 reproducibility on lead ratios is around 100 ppm. Blanks are typically lower than 20 pg.

5 Results

5.1 Major and trace elements

The mafic volcanic rocks totals vary in the range 98.28 to 101.82 wt% with an average of 100.46 wt%. Most samples contain

180 less than 3 wt% LOI (loss on ignition), an indication of the reliability of their geochemistry (i.e., the rocks have maintained their original geochemical characteristics; see the subtitle Alteration in Discussion section). On Harker variation diagrams, CaO, MgO, and FeO^t show broadly decreasing trends with increasing SiO$_2$ whereas Na$_2$O and K$_2$O increase (Fig. 2). These covariations are well defined for specific areas (cf. Figs. 2 and S3 a, b). Volcanic rocks from Marbin and Kahang show higher Mg and Ca and lower Fe, Na, and K compared to the Fordou and Vadghan areas (cf. Figs. S3.a, b). These largely correspond

185 to the volcanic rocks from the LILE-poor and LILE-rich series (see below) respectively.

The mafic volcanic rocks from the study area can be divided into three distinct compositional series based on their primitive mantle (Sun and McDonough, 1989) normalized trace element patterns. On Fig. 3 these are termed the LILE-poor, the LILE-rich, and the ITE-rich series (LILE and ITE refer to large-ion lithophile elements and incompatible trace elements respectively). The LILE-poor and LILE-rich series show negative Nb-Ta anomalies, which clearly favour an arc setting. These rocks belong

190 to the subalkaline series and further show calc-alkaline affinities. The LILE-poor series is rather depleted in Rb, K, and HREE compared to the LILE-rich series. The ITE-rich series is enriched in the lithophiles, La, Ce, Pb, Sr, and P with both calc-alkaline and alkaline features. Mafic volcanic rocks from the ITE-rich series are sometimes enriched in Nb-Ta (Fig. 3; diagrams in the upper row).

Volcanic rocks exhibiting these three patterns (i.e., the LILE-poor, LILE-rich, and ITE-rich series) also show some major

195 element geochemical distinctions. Rocks from the LILE-poor series show higher Mg and Ca and lower Fe, and alkaline elements as compared to the LILE-rich series samples (Figs. 2 and S3.a-c). Details of the mafic rock variation diagrams for

three segments of the study area are shown in Fig. S3.a-c; these are Kahak (Fodou and Vadghan), Ardestan (Mishab, Marbin, and Kahang), and Nodoushan (Fig. 1). Importantly, the mafic volcanic rocks of the three series/patterns occur across all segments of the study areas, though vary in their different proportions.
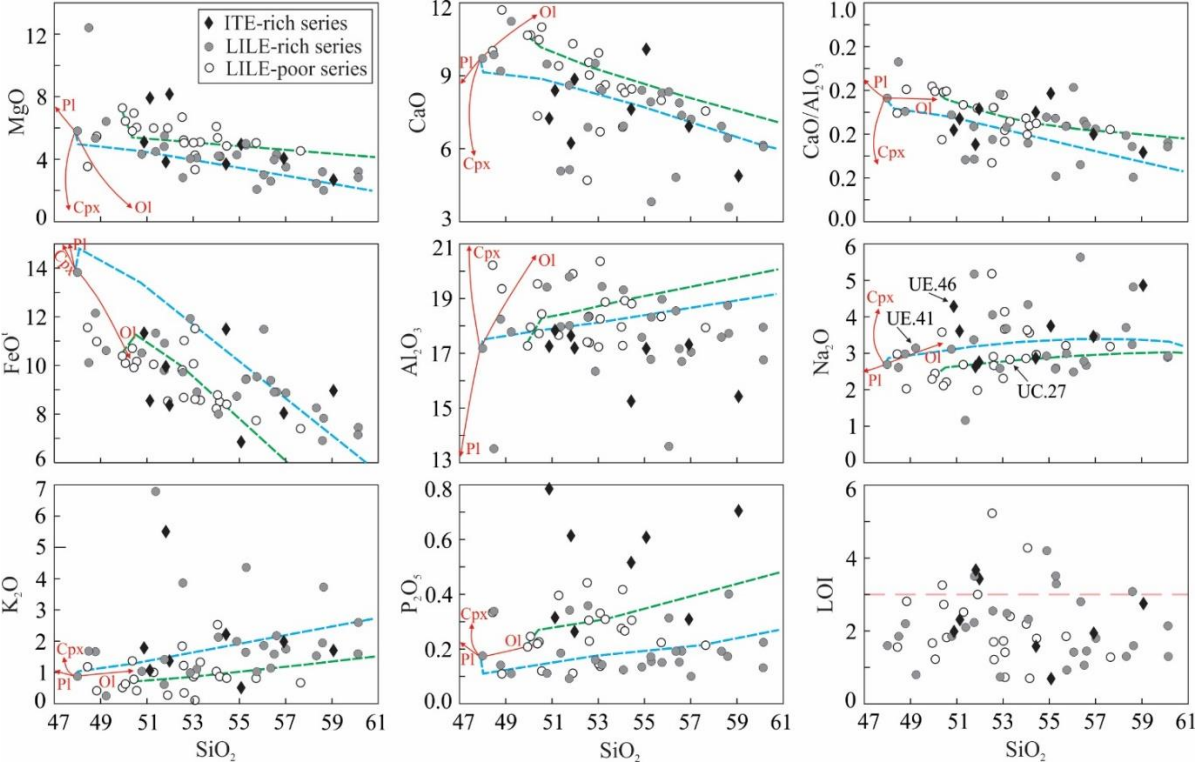
Figure 2: Major element oxides vs. SiO₂ variation diagrams for the LILE-poor, LILE-rich, and ITE-rich series from the UDMA. For details of the variation diagrams also see Figs. S3.a-c. The red solid lines with arrows indicate the effect of 20% fractional crystallization of olivine (Ol), clinopyroxene (Cpx), and plagioclase (Pl) on the whole-rock compositions (calculated using MagPath spreadsheet software; Mayborn and Lesher, 2011). Blue dashed line is the calculated liquid line of descent by 83% fractional crystallization of 0.18 olivine + 0.41 clinopyroxene + 0.40 plagioclase + 0.01 apatite, followed by 17% fractional crystallization of 0.05 olivine + 0.31 clinopyroxene + 0.48 plagioclase + 0.16 Ti-magnetite. Green dashed line denotes the calculated liquid line of descent by 75% fractional crystallization of 0.25 olivine + 0.41 clinopyroxene + 0.33 plagioclase + 0.01 Ti-magnetite, followed by 25% fractional crystallization of 0.06 olivine + 0.32 clinopyroxene + 0.46 plagioclase + 0.16 Ti-magnetite. The blue and green dashed lines, the calculated liquid lines of descent, match well with the trend defined by natural samples from the LILE-rich and LILE-poor series respectively. These FC models imply that the LILE-poor and LILE-rich series were derived from different parental magmas.
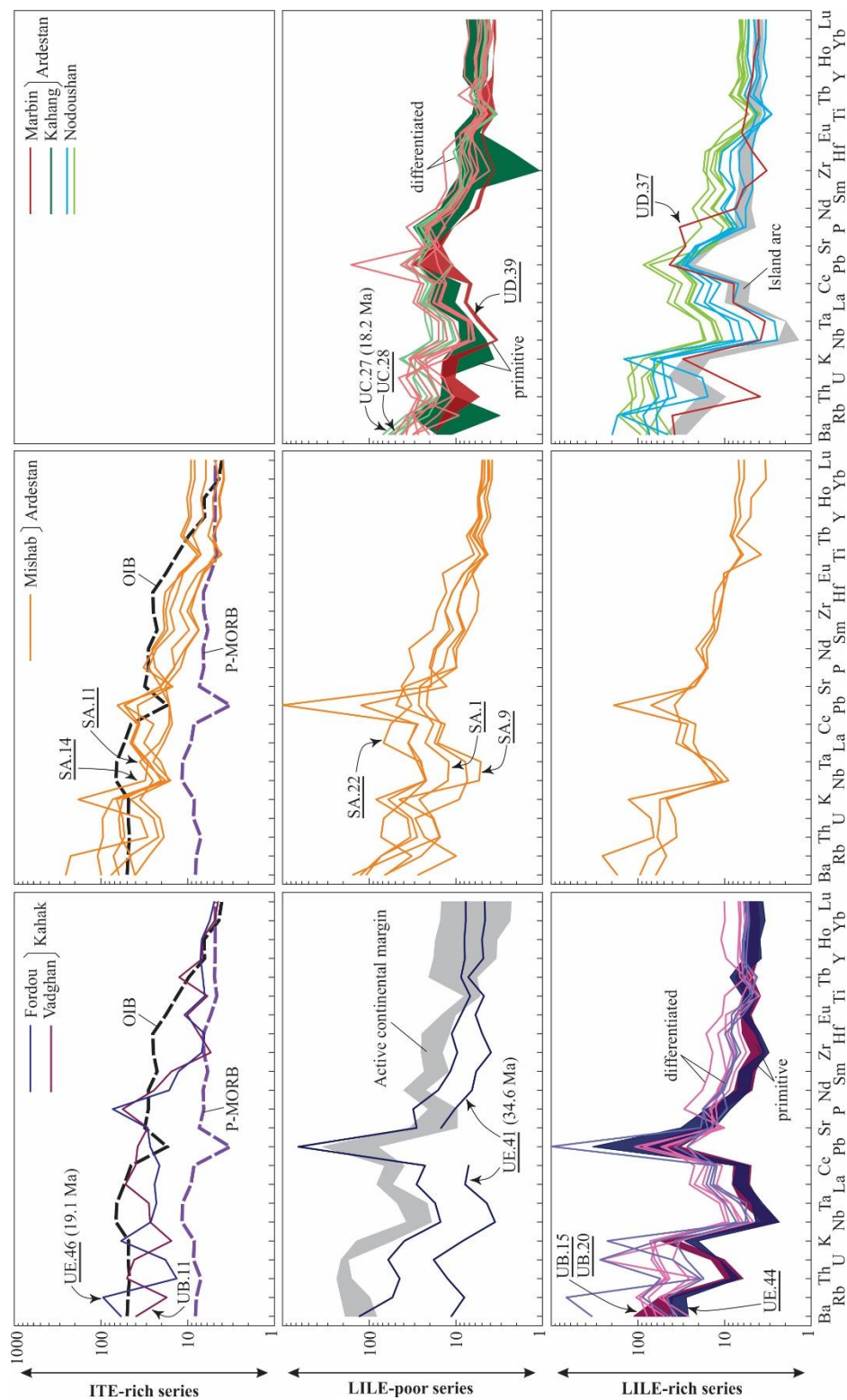
Figure 3: Primitive mantle normalized trace element patterns for the Kahak (including Fordou and Vadghan), Ardestan (including Mishab, Marbin, and Kahang), and Nodoushan mafic volcanic rocks. These are classified into the LILE-rich, LILE-poor, and ITE-rich series. Differentiated samples are shown in pale colours as compared to the more primitive samples which are shown in dark colours. Underlined sample numbers indicate the mafic volcanic rocks for which Sr-Nd-Pb isotopic data were obtained in the current study (see Table S3 and Fig. 4). Age-dated samples are from Ghorbani et al. (2014). For other age-dated samples from the study areas see Figs. S4 and S5. Primitive mantle (PM) normalization values and trace element abundances for the OIB and P-MORB (diagrams in the upper row) are from Sun and McDonough (1989). Trace element abundances for the island arc basalts (lower right diagram) and active continental margin basalts (middle left diagram) are from Jicha and Singer (2006) and Straub et al. (2015) respectively.

5.2 Sr-Nd-Pb isotopic data

Sr-Nd-Pb isotopic ratios were determined for a set of fourteen mafic volcanic rocks (Table S3) from the study areas belonging to the LILE-rich series (four samples), the LILE-poor series (six samples) and the ITE-rich series (four samples). The ranges of measured Sr isotopic ratios for these three series are 0.70562 to 0.706085, 0.705099 to 0.706263, and 0.704443 to 0.705561 respectively. The ranges of measured Nd isotopic ratios for these three series are 0.512715 to 0.512786, 0.512607 to 0.512766, and 0.512673 to 0.512804 respectively.

Only four out of the fourteen samples are age-dated using the whole rock K-Ar method (Ghorbani et al., 2014). These range from 18.2 to 34.6 Ma, similar to the ages obtained for the UDMA mafic volcanic rocks by Yeganehfar et al. (2013). None of the three series of volcanic rocks (the LILE-rich series, the LILE-poor series, and the ITE-rich series) appear to be confined to a particular time span. Mafic volcanic rocks of the same compositional affinities from the central UDMA studied by Moradi et al. (2021) further extended this age range from 21.5 to 60.0 Ma. Therefore, an average age of 35 Ma is suggested for calculation of the initial Sr, Nd, and Pb isotopic ratios. The ranges of initial Sr isotopic ratios for these three series are 0.705448 to 0.706017, 0.705044 to 0.706237, and 0.704379 to 0.705505 respectively. The ranges of initial Nd isotopic ratios for these three series are 0.512677 to 0.512746, 0.512573 to 0.512729, and 0.512637 to 0.512772 respectively (Table S3).

The mafic volcanic rocks from the study area plot on the same area of the Sr-Nd isotopic plot as other orogenic volcanic rocks and on the same area as other mafic volcanic rocks from the UDMA (Fig. 4). Toward lower Sr isotopic ratios, data points from the three series converge to share a narrow space in the mantle array close to the Bulk Silicate Earth (BSE). The Sr-Nd isotopic variation trends expand towards higher Sr and lower Nd isotopic ratios (Fig. 4.a). These volcanic rocks display moderately radiogenic Pb compositions ($^{206}Pb/^{204}Pb_{(i)}$ = 18.52-18.72, $^{207}Pb/^{204}Pb_{(i)}$ =15.51-15.69, and $^{208}Pb/^{204}Pb_{(i)}$ = 38.33-38.80; Table S3). On Pb-Pb isotopic plots, the mafic volcanic rocks form linear trends stretching from the mantle array (i.e., NHRL) towards enriched mantle that is above the reference line (Fig. 4.b, c).
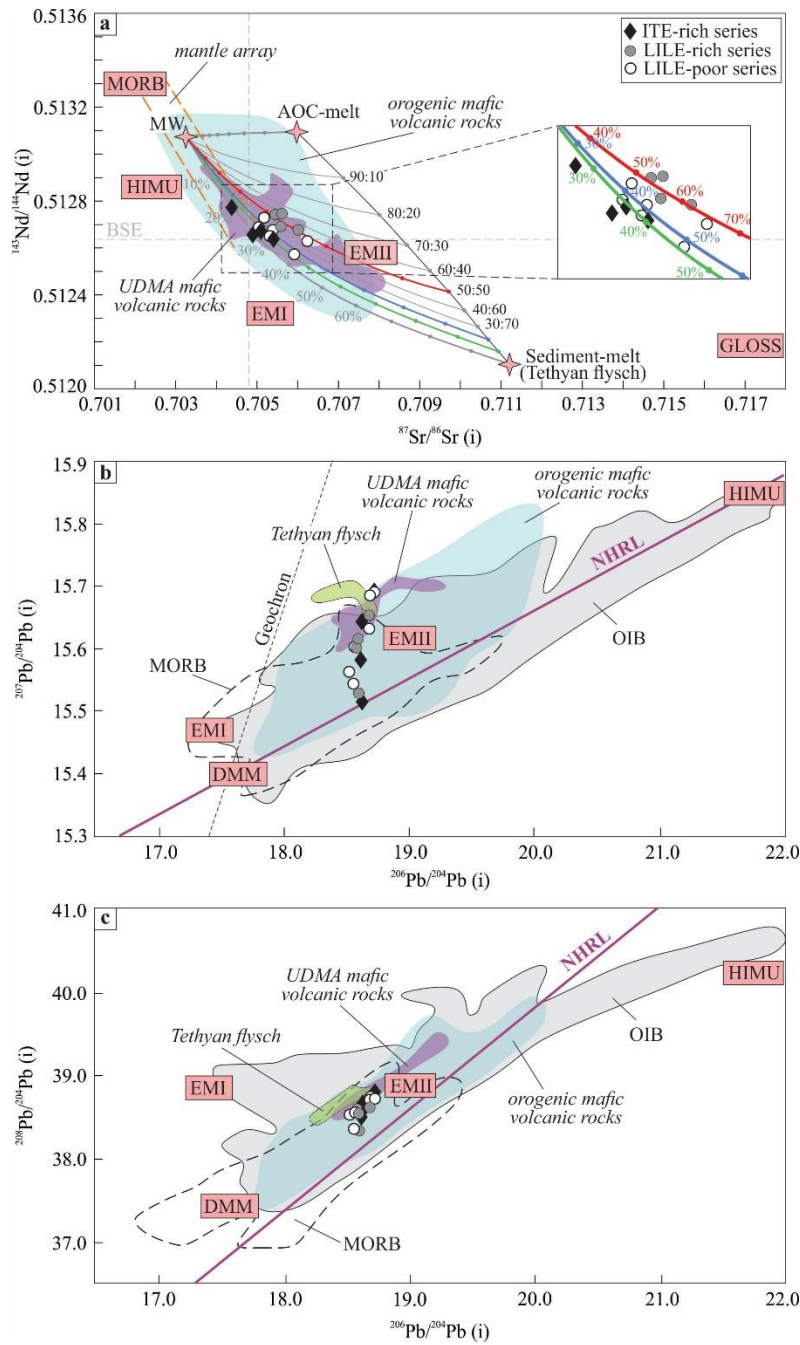
Figure 4: (a) Initial Sr-Nd isotopic ratios plot for the mafic volcanic rocks from the study areas, showing a three-component mixing model, determined using a simple mass-balance approach (Powell, 1984), for the LILE-rich, LILE-poor, and ITE-rich series mafic volcanic rocks from the central UDMA. See Supplementary Table S5 for further details on modelling parameters. (b) ^{207}Pb/^{204}Pb vs. ^{206}Pb/^{204}Pb and (c) ^{208}Pb/^{204}Pb vs. ^{206}Pb/^{204}Pb ratios plots for the mafic volcanic rocks from the study areas. Average values for DMM (depleted MORB mantle), HIMU (high µ; µ = ^{238}U/^{204}Pb), EMI (enriched mantle 1), and EMII (enriched mantle 2) are calculated

250

based on the samples presented in Akbari et al. (2023) that include a comprehensive database on a variety of basalts. GLOSS (global subducted sediment) is adapted from Plank and Langmuir (1998). The fields for OIB (oceanic island basalts) and MORB (mid-ocean ridge basalt) are from Stracke et al. (2003, 2005), Chauvel et al. (2008), and references therein. NHRL (Northern Hemisphere Reference Line) is adapted from Hart (1984). The mantle wedge is represented by the average of Kamchatka arc volcanic rocks (Kepezhinskas et al., 1997), the altered oceanic crust (AOC) is adopted from Hauff et al. (2003), and the Tethyan flysch sandstone sample 06FL03 from Serbia is adopted from Prelević et al. (2008). For comparison of the data achieved in the present study with published isotopic data for the W Nain (Yeganehfar et al., 2013) and Nodoushan (Jolani Varzeghani, 2017) areas see Fig. S6. The field for orogenic mafic volcanic rocks is adapted from the GEOROC database. The distribution of nearly coeval mafic volcanic rocks from UDMA (Omrani et al., 2008; Yeganehfar et al., 2013; Shafaii-Moghadam et al., 2014; Jolani Varzeghani, 2017; Khodami, 2019; Rabei et al., 2020; Moradi et al., 2021) are also shown for comparison. See text for more details.

6 Discussion

6.1 Alteration

The development of secondary minerals in the mafic volcanic rocks from the study areas is strictly limited to a few pseudomorphs after primitive olivine and orthopyroxene (see Section 3, Petrographic analysis). This along with LOI values lower than 3 wt% in most of the samples (i.e., in 55 out of 66 samples) indicates negligible alteration effects. In addition, most of the samples from the LILE-poor series have the same LOI abundances as the samples from the LILE-rich series (Figs. 2 and S3.a-b). These overlapping volatile contents do not support a correlation between the LOI and alkali contents (see Fig. 2) which is usually regarded as a measure of the extent of alteration (e.g., Dong et al., 2017). In Mishab, the LILE-poor series samples have the highest LOI (Fig. S3.a); this does not support a correlation between alkali content and LOI and provides yet additional evidence as to the lack of significant alteration effects.

6.2 Primitive signatures

Mafic magmatic rocks are not common in magmatic arcs (e.g., Plank and Langmuir, 1988). Subduction or arc-related volcanic successions are dominated by the intermediate to felsic volcanic products and these are conventionally viewed as derivatives of arc basaltic magmas which have been triggered by partial melting of metasomatic components in the mantle wedge (Gill, 1981; Plank and Langmuir, 1988; Benoit et al., 2002; Streck et al., 2007). A thick continental lithosphere and/or crust promotes the development of high-level magma chambers that prohibit rapid magma ascent and leads to significant magmatic differentiation, namely Assimilation − Fractional Crystallization (AFC), and this masks most of the original source mantle signatures (Plank and Langmuir, 1988; Farner and Lee, 2017). MgO contents of the volcanic rocks from the study area are rather low (< 7 wt%) indicating that even the most mafic samples experienced some degrees of differentiation. It is however noted that some of the least differentiated samples from magmatic arcs maintain the trace element signatures of primitive melts. As a measure of the rather primitive nature of the volcanic rocks, their Mg# are presented in Table S2. Non-cumulative,

rather aphyric or slightly porphyritic UDMA mafic rocks with low LOI contents and minor or no alteration, are examined here to infer implications as to the geochemical signatures of their primitive melts.

It is noted above that the mafic volcanic rocks from the study area are representative of three distinct trace element patterns, namely the LILE-poor, LILE-rich, and ITE-rich series. Samples from the LILE-poor and LILE-rich series are marked by a distinctive negative Nb-Ta anomaly, characteristic of subduction-related settings (Fig. 3; see lower right and middle left diagrams for island arc and active continental margin volcanic rock trace element patterns respectively). The LILE-poor series are depleted in the lithophiles whereas the LILE-rich series are enriched in the lithophiles. The trace element pattern for the ITE-rich series is significantly different; it is enriched in the lithophiles, La, Ce, Pb, Sr, and P. Samples from the ITE-rich series are rather enriched in Nb-Ta and present OIB-like trace element patterns (Fig. 3; diagrams in the upper row).

The LILE-poor and LILE-rich series trace element patterns span a wide spectrum from an overall low trace element abundance to an overall high/elevated trace element abundance. The patterns with an overall low trace element abundance (i.e., of < 10 times primitive mantle) show less differentiated signatures (e.g., slight or no negative Sr and Ti anomalies) and are suggested to represent more primitive partial melts. The low trace element abundance patterns are likely to imply high-degree partial melts (Wilson, 1989). Higher-degree partial melts show lower trace element abundances as well as evidence supporting the exhaustion of fusible mantle mineral phases (Ghorbani and Middlemost, 2000). A pronounced negative anomaly in Zr-Hf in some of the UDMA mafic volcanic rocks with an overall low trace element abundance pattern (Fig. 3) appears to indicate the significant contribution of a mineral phase that bears a negative Zr-Hf anomaly. The gradual consumption and final disappearance of clinopyroxene in the mantle source, as the major participating phase, could impose such a low Zr-Hf signature (Linnen and Keppler, 2002; Atanasova et al., 2020) on the partial melt produced. Alternatively, it may indicate metasomatism by slab partial melts in the source mantle of the LILE-poor series. Metasomatism by slab partial melts is associated with the development of Al-rich orthopyroxene and Mg-rich amphibole in the mantle (Schiano et al., 1995; Kepezhinskas et al., 1995; Szabó et al., 2004). This contracts the clinopyroxene (Cpx) stability field so that the LILE-poor series parental melts portray signatures of Cpx exhaustion.

Most of the mafic volcanic rocks from the study area show large negative anomalies for Th but mild or no anomaly for U, similar to island arc volcanics (Hawkesworth et al., 1997). This is because Th behaves like HFSE whereas U is mobilised by fluids. However, a few samples from the LILE-poor series show positive Th-U anomalies (Fig. 3). One of these samples shows the highest LREE and P abundances amongst the mafic volcanic rocks (sample SA.22; Fig. 3). These may indicate apatite involvement in the petrogenesis of the mafic volcanic rocks with positive Th-U anomalies. Apatite shows extremely high partition coefficients for Th, U, and LREE (O'Reilly et al., 1991). Morishita et al. (2003) found that apatite development in the Finero peridotite is due to a metasomatizing agent derived from subducting 'slab possibly containing small quantity of sediment', a condition supported by the isotopic modelling of source end-members for the mafic volcanic rocks from the study area (see Section 6.6).

6.3 Does fractional crystallization provide an interseries link?

The fact that two series of the samples with the most primitive geochemical signatures (i.e., from the LILE-poor and LILE-rich series) show significant differences in LILE implies that the differences/distinctions are source-inherited. In other words, more primitive samples from these two series best represent their compositional distinctions. Hence, the LILE-poor and LILE-rich series are likely rooted in different source regions. One might challenge this hypothesis and assign the geochemical differences between the two series to differentiation from a single parental melt. Fractionation of the liquidus phases crystallizing from primary mafic melts (i.e., Ol, Opx, Cpx, and Pl; a single phase or a mineral assemblage) may explain some geochemical differences between the two series. Fractionation of Ol + Pl ± Cpx from an assumed primary mafic melt can explain the major element geochemical evolution from the LILE-poor series to the LILE-rich series rocks (i.e. decreasing melt Mg and Ca, and increasing Fe and alkaline elements). However, this model is not able to explain the distinction/differences between the trace element abundances and patterns of the two series. Such a differentiation model is expected to produce a series of parallel trace element patterns wherein the abundances of nearly all incompatible trace elements (i.e., with the exception of P and Sr due to the fractionation of apatite and plagioclase, respectively) increase as differentiation proceeds. Moreover, the differentiation model is not able to explain some other issues as follows: 1- negative Th anomalies of the LILE-rich series samples are not consistent with their more differentiated nature. Th is a highly incompatible element and is expected to increase with differentiation. Although Th can be compatible in apatite, the rather constant and minimal P_2O_5 abundances in the LILE-rich series do not support apatite fractionation. 2- the volcanic rocks representing the LILE-poor and LILE-rich series stretch parallel to each other across the compositional spectrum at the same silica range (Fig. 2). This is more consistent with the concurrent evolution of two series rather than one being the differentiation product of the other.

As noted above, the LILE-poor and LILE-rich interseries geochemical differences are unlikely to have been interconnected (i.e., the latter is not developed by differentiation of the former). Rather, the two series bear some primitive signatures and are likely derived from two distinct source mantle regions. Nevertheless, the LILE-poor and LILE-rich intraseries geochemical variations appear to have been developed by differentiation through fractional crystallization (FC). The intraseries FC model is supported by the following five observations: 1- The presence of Ol, Opx, Cpx, Pl, and Fe-Ti oxides phenocrysts in the UDMA volcanic rocks. 2- The development of elevated, parallel trace element patterns in the more evolved samples of the respective series (i.e., the LILE-poor and LILE-rich series; Fig. 3). 3- The gradual decrease of some trace elements which have high Kd for the fractionated minerals (e.g., development of negative Ti anomaly) in the more evolved samples. 4- The plots of differentiation index versus the Sr and Nd isotopic ratios confirm the dominance of FC with little or no crustal contamination in the evolution of the volcanic rock series from the study area (Fig. 5; for details on the one sample from ITE-rich series and two samples from the LILE-poor series that are marked with arrows and show different geochemistry as compared to the mainstream respective series, see Sections 6.5 and Fig. 5 caption respectively). 5- Fractional crystallization modelling using the MagPath algorithm (Mayborn and Lesher, 2011) demonstrates different liquid lines of descent for the LILE-rich and LILE-poor series, developed as a result of differentiation of distinct mineral assemblages (see Fig. 2 caption for details). Pb isotopic

ratios as more sensitive tools for the detection of crustal components however, indicate some crustal contamination. Decreasing 350 $^{207}Pb/^{204}Pb$ with increasing silica (Fig. 5) for most samples indicates interaction with unradiogenic lower crust.
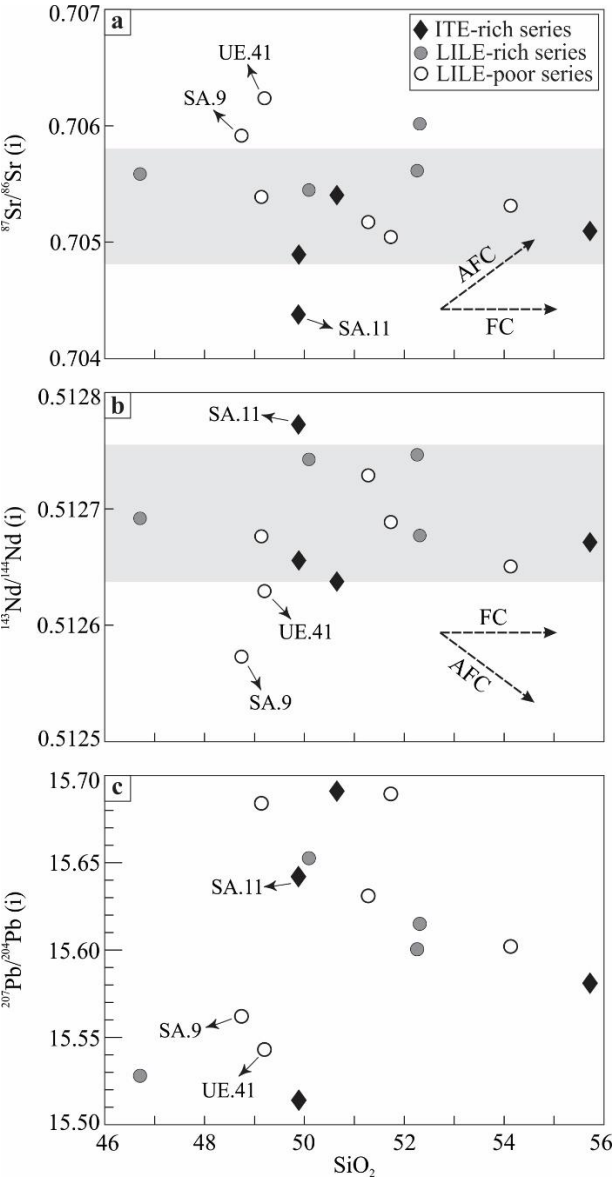
Figure 5: Plots of (a) $^{143}Nd/^{144}Nd_{(i)}$, (b) $^{87}Sr/^{86}Sr_{(i)}$, and (c) $^{207}Pb/^{204}Pb_{(i)}$ vs. SiO$_2$, as a fractionation index, for the LILE-rich, LILE-poor, and ITE-rich series mafic volcanic rocks from the central UDMA; details in the text. Gray areas/bands marks restricted Sr-
355 **Nd isotopic variation for most of the mafic volcanic rocks. One sample from the ITE-rich series plots towards less radiogenic Sr-Nd isotopic ratios (see Section 6.5 and Fig. 4.a for details). Two samples from the LILE-poor series plot towards more radiogenic Sr-Nd isotopic ratios; this is due to the higher slab components (i.e., slab + sediment) involvement (see Section 6.6 and Fig. 4.a).**

Mafic volcanic rocks with the most primitive geochemical signatures are presented in the current study. Further assurance as to the primitive nature of the ternary classification of the volcanic rocks from the study area (i.e., that the geochemical distinction between these three rocks series are not the artefact of fractional crystallization) are provided by a series of plots where mafic samples define distinct groupings/series. SiO_2 versus Ba/Nb or Ba/La help distinguish the LILE-rich from the LILE-poor series (Fig. 6.a, b) whereas SiO_2 versus Nb or Zr help distinguish the ITE-rich series from the other two series (Fig. 6.c, d). However, Nodoushan volcanic rocks contain >54% silica and are rather differentiated. This is indicated by the Nodoushan rocks having pronounced negative anomalies for Ti and P as well as their elevated trace element patterns (Fig. 3). In fact, Nodoushan rocks constitute two sets of compositional variations, samples with larger negative Sr anomalies (i.e., the more differentiated set) are richer in incompatible trace elements as compared to the more primitive set. In Fig. 3 these are shown by green and blue patterns respectively. The more differentiated set shows lower Al abundances attesting to the higher degree of plagioclase differentiation (Fig. S3.b).
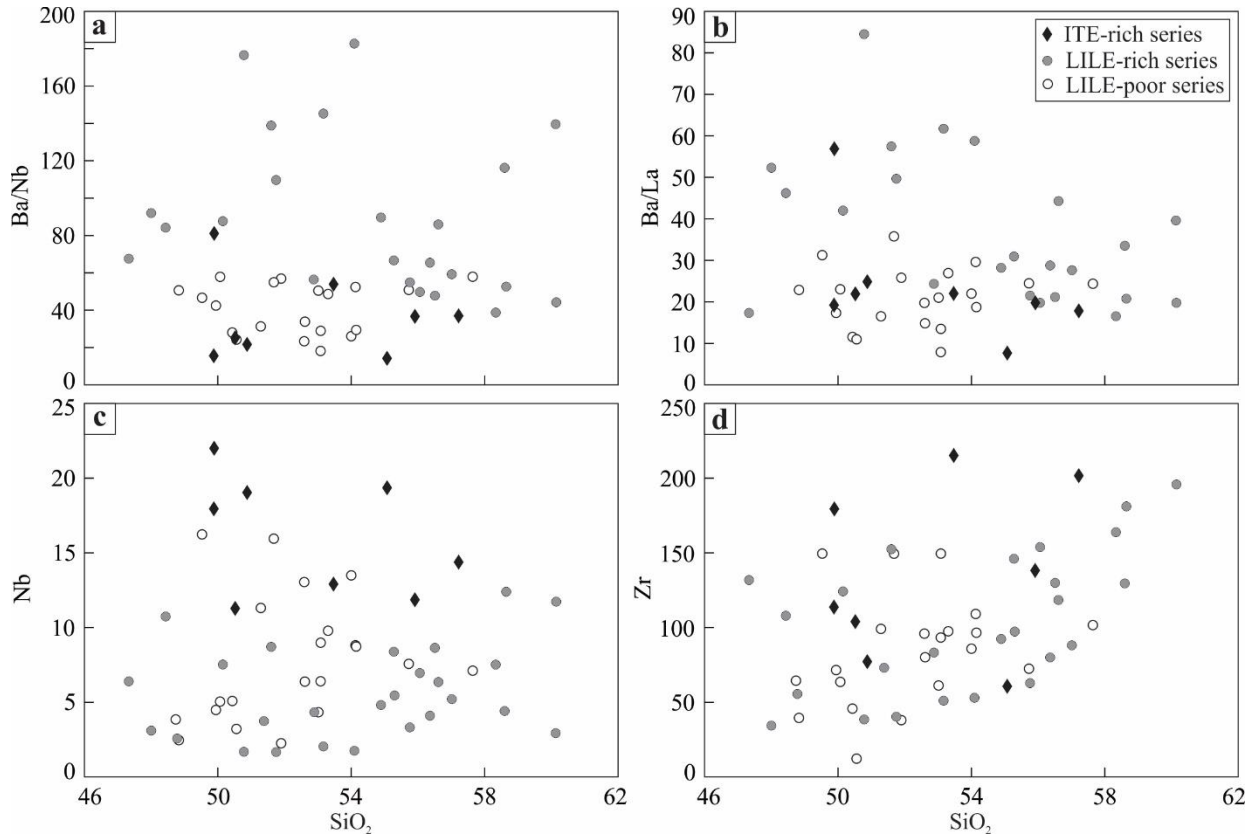
Figure 6: SiO_2 versus (a) Ba/Nb, (b) Ba/La, (c) Nb, and (d) Zr plots used for discrimination of LILE-rich, LILE-poor, and ITE-rich series (see text for details).

375 **6.4 Mantle metasomatism by fluid-rich slab melts and fluid-poor slab melts; furnishing sources of the LILE-rich and LILE-poor series respectively**

Different modes of trace element enrichment (i.e., by fluids/melts released from the subducting slab) in the source mantle may be responsible for the development of the LILE-poor and LILE-rich series melts. Melting of the mantle metasomatized by fluid-rich-slab-melt is suggested to have produced the LILE-rich series melts whereas melting of the mantle metasomatized

380 by the partial melt of the same but dehydrated slab segment (i.e., fluid-poor-slab-melt), is likely to have led to the LILE-poor series melts. This is consistent with the more Mg-rich composition of the latter (Fig. 2). This occurs because the mantle with lower lithophiles and volatiles, has a higher solidus and is more magnesian in composition (Pickering-Witter and Johnston, 2000).

The contribution of more fluids in the evolution of the LILE-rich series is implied by the trace element ratio plots (Fig. 7). The

385 phase equilibria relation is also in line with this model (i.e., fluid-rich-slab-melt versus fluid-poor-slab-melt involvement in the petrogenesis of the LILE-rich and LILE-poor series respectively). Higher mobile incompatible element abundances of the primitive melt in the LILE-rich series are consistent with the geochemical evolution of the LILE-rich series; that is the hydrous nature of the LILE-rich primitive melt depressed plagioclase fractionation and thereby prompted an early Al increase in the 48-52 wt% silica range in the series. Two different scenarios are raised here that may account for the petrogenesis of these two

390 major rock series.
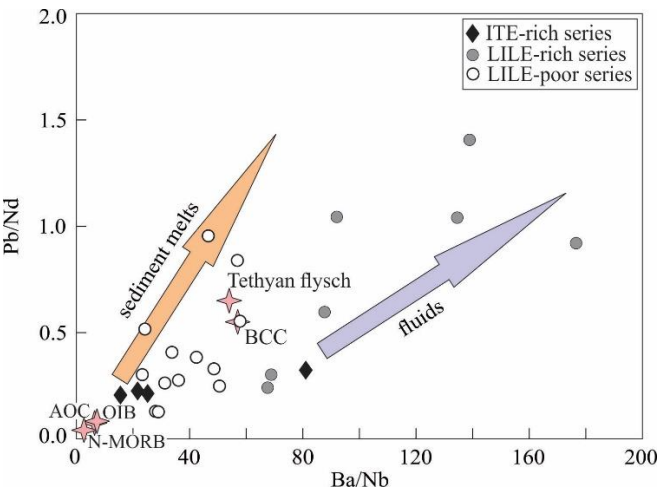
Figure 7: Ba/Nb versus Pb/Nd plot for the mafic volcanic rocks (SiO$_2$ < 52 wt%) from the study area. Higher mobile/immobile trace elements ratios in the LILE-rich series indicate the involvement of higher fluid in the petrogenesis of this series (e.g., Duggen et al.,

395 **2007; Straub et al., 2015). For references of the components involved (OIB, N-MORB, AOC, Tethyan flysch) see the caption for Fig. 4.**

6.4.1 The slab roll-back scenario

Considering the emphasis that has recently been made in regard to the application of the slab roll-back model in the petrogenesis of the Cenozoic magmatic arc of Iran (Agard et al., 2005; Verdel et al., 2011; Yeganehfar et al., 2013; Babazadeh et al., 2017; Moradi et al., 2021), one may prompt a two-stage mantle metasomatism model as being responsible for the petrogenesis of the two series of volcanic rocks from the study area as follows. Slab dehydration at a given depth produced the 'lithophile enriched' source mantle that generated the LILE-rich series melts. Gradual deepening (or roll-back) of the dehydrated, lithophile-depleted slab, was associated with an increasing temperature that prompted partial melting of the slab. This slab melt was depleted in lithophiles but enriched the overlying mantle in 'immobile, highly incompatible elements'. Due to the involvement of slab partial melts, the LILE-poor series melts are enriched in the immobile trace elements Nb to P (i.e., on the normalized trace element patterns; Fig. 3) as compared to the LILE-rich series. This scenario however, does not stand up to close scrutiny. A review of the age-dated mafic volcanic rocks from the study area (Ghorbani et al., 2014; see Fig. 3) and nearby areas (Ghorbani and Bezenjani, 2011; Yeganehfar et al., 2013; see Figs. S4 and S5) do not indicate that the LILE-poor series postdate the LILE-rich series.

6.4.2 Simultaneous fluid-rich slab melts and fluid-poor slab melts mantle metasomatism scenario

It is suggested here that the fluid-rich-slab-melt and the fluid-poor-slab-melt metasomatism, leading to the development of the LILE-rich and the LILE-poor series, took place concurrently or in a short time span along the entire magmatic arc. Young hot slabs are capable of yielding partial melts at sub-arc depths that correspond to the volcanic front (Hermann and Spandler, 2008; Manea et al., 2014; Zheng, 2019). Hot slab subduction of a then narrow/almost vanished Neotethyan oceanic plate has likely been responsible for petrogenesis of the slab melts that metasomatized source mantles of the three rock series; the LILE-rich, LILE-poor, and ITE-rich series. Disappearance and termination of the Neotethyan oceanic slab is estimated to have predated the early Cenozoic (Agard et al., 2005; Horton et al., 2008; Dargahi et al., 2010). The LILE-rich and LILE-poor series rocks are mainly spatially constrained in occurrence towards the northern and central parts of the study area, namely the Kahak and Ardestan areas respectively. This implies a more hydrated, more altered nature of the northern segment of the slab subducting in the Kahak area whereas the segment of the slab subducting in the Ardestsan area is deemed to have been of a higher T (i.e., they may have been thicker and thinner slabs respectively).

6.5 The incompatible trace element-rich (ITE-rich) series (including OIB-like samples)

Samples from the ITE-rich series are enriched in a wide range of incompatible trace elements that include lithophiles, La, Ce, Pb, Sr, and P, so they are called the incompatible trace elements-rich series, or ITE-rich series (Fig. 3). These include the most Nb-Ta enriched samples from the study area that approach the OIB pattern and therefore may be called OIB-like samples. However, they are not genuine OIBs as; 1) their trace element patterns are rather differentiated (i.e., as compared to the smooth trace patterns of the OIBs; Fig. 3), 2) their trace element abundances are not as high as OIBs, and 3- their Sr-Nd-Pb isotopic

signatures partly overlap those of the LILE-rich and LILE-poor series (Fig. 4). However, Sr and Nd isotopic ratios for the ITE-rich series extend towards lower and higher values respectively (i.e., as compared to the LILE-rich and LILE-poor series). Samples from the ITE-rich series are more like high-Nb basalts (HNBs; Defant et al., 1992). The occurrence of HNBs in the subduction framework is attributed to either a mantle plume (i.e., an asthenospheric or OIB-type mantle) or a metasomatized mantle wedge (Reagan and Gill, 1989; Castillo et al., 2007). The HNBs are also known to be the mixing products of an enriched (e.g., OIB-type) and a depleted (e.g., arc-type) source mantle (Hastie et al., 2011; Ahmadvand et al., 2021; Akbari et al., 2022). The ITE-rich series is suggested to have been generated by a slab-window or slab-tearing process at moderate pressures whereby the underlying asthenospheric mantle penetrated into and facilitated slab partial melting that interacted with and metasomatized the mantle to produce the ITE-rich series (Benoit et al., 2002). The OIB trace element pattern for sample SA.11 from the ITE-rich series (Fig. 3) supports asthenospheric mantle involvement. On the Sr-Nd isotopic plot this sample deviates further towards and plots within the mantle array as compared to the other samples from the ITE-rich series (see caption in Fig. 5).

6.6 Slab/crustal contributions to the arc magmatism

As differentiation by fractional crystallization (FC; see above) proceeds in a magmatic series, the more evolved melts show higher abundances of incompatible trace elements (e.g., Zheng, 2019). This is because the fractionated mineral assemblage has low Kd for the incompatible trace elements. However, in some batches of differentiated samples, the spate of increasing abundances of a few incompatible trace elements such as Th, K, La, and Ce, exceeds that of the other incompatible trace elements. These are believed to indicate crustal contamination or assimilation which is usually associated with FC (i.e., assimilation – fractional crystallization, AFC). Arc mafic volcanic rocks, due to the rather high ascent rate of mafic melts, are less likely to have undergone significant continental crustal contamination. Hence, their crustal signatures have probably been derived from the slab (i.e., slab plus sediment) fluids and melts that metasomatized the overlying mantle wedge (e.g., Benoit et al., 2002).

The origin and evolution of mafic volcanic rocks are best represented by the Sr-Nd-Pb isotopic ratios. The three series of volcanic rocks from the UDMA (i.e., the LILE-poor, LILE-rich, and ITE-rich series) plot on the same area of the Sr-Nd isotopic plot as other orogenic volcanic rocks and on the same area as other mafic volcanic rocks from the UDMA (Fig. 4). However, subtle but significant differences are observed in the distribution of the three series on this plot. Towards lower Sr isotopic ratios, data points of the three series converge to share a narrow space in the mantle array close to the BSE. The Sr-Nd isotopic variation trends expand towards higher Sr and lower Nd isotopic ratios (Fig. 4.a). Increasing Sr isotopic ratios occur at constant Nd isotopic ratios in the LILE-rich series whereas in the LILE-poor and ITE-rich series, the Sr isotopic ratios increase with decreasing Nd isotopic ratios (Fig. 4.a).

On Pb-Pb isotopic variation diagrams (Fig. 4.b, c) the least radiogenic members of the three series of mafic volcanic rocks, the LILE-poor, LILE-rich, and ITE-rich series, plot on the DMM-OIB mantle array (i.e., on the moderately depleted mantle area of the NHRL). The more differentiated volcanic rocks demonstrate sharp enrichment trends towards radiogenic Pb end-

members on the Pb-Pb isotopic plots. Interestingly, the three series of volcanic rocks share one variation trend on these plots; this means that the fluid-rich-slab-melt and fluid-poor-slab-melt (i.e., responsible for development of the LILE-rich and LILE-poor series respectively) maintain the same Pb isotopic ratios. This implies that, unlike different LILE/MREE ratios in the slab components involved in the petrogenesis of the LILE-rich and LILE-poor series, these slab-derived components have the same U content and U/Th ratio.

It was noted above that the geochemistry does not support continental crustal contamination (see Fig. 5). The isotopes are not fully discriminant to support the trace element classification of mafic volcanic rocks into the three series presented here. However, the isotopes may be utilized to evaluate/estimate the geochemical reservoirs involved in their petrogenesis. Assuming a negligible continental crustal contamination in the evolution of the UDMA mafic volcanic rocks and utilizing the Sr-Nd isotopic data, ternary mixing modelling was carried out and shows that the UDMA mafic volcanic rocks can be best explained by mantle wedge and slab (i.e., including slab melt and sediment melt) participation.

The mantle wedge, slab and slab sediment are respectively represented by the average of Kamchatka arc volcanic rocks (Kepezhinskas et al., 1997), altered oceanic crust (AOC; Hauff et al., 2003), and the Tethyan flysch sandstone sample 06FL03 from Serbia (Prelević et al., 2008). The ternary mixing model applied for the UDMA mafic rocks found that in the LILE-rich and LILE-poor series, mantle wedge:slab contributions were 45:55 and 55:45 respectively. Numbers marked on the red and blue mixing curves in the inset of Fig. 4a indicate that slab involvement in the petrogenesis of the LILE-rich and LILE-poor series was 50-60% and 40-50% respectively. For simplicity these are presented as mean values of 55% and 45%. The green curve is not recommended as a mixing model for the development of the ITE-rich series. As mentioned earlier, the ITE-rich series has likely been generated in a process similar to the one that led to the high-Nb basalts (Section 6.5).

Intercept of the red and blue mixing curves with the slab melt-slab sediment array marks the proportion of slab melt:sediment melt involved in the petrogenesis of the LILE-rich and LILE-poor series (i.e., 50:50 and 20:80) respectively. Combining these two figures, mantle wedge:slab melt:sediment melt proportions of 45:27.5:27.5 and 55:09:36 are obtained for the LILE-rich and LILE-poor series respectively. Mafic volcanic rocks from the W Nain area of the central UDMA (Yeganehfar et al., 2013) with trace element patterns that mimic the LILE-rich, LILE-poor, and ITE-rich series patterns (Fig. S5) show Sr-Nd-Pb isotopic characteristics that are similar to the respective series from the study area, further supporting the petrogenetic model presented here (Fig. S6).

Although the least evolved mafic volcanic rocks from the UDMA are presented in this study, volcanic rocks from the Nodoushan (i.e., southeastern segment of the study area) are still highly differentiated (see Section 6.3 and Fig. S3.b). The Nodoushan rocks also show significant crustal contamination signatures such as elevated lithophiles, Th, Pb, La-Ce, and Sr isotopic ratios. Some of the volcanic rocks show the highest Sr isotopic ratios from the study area. Hence, they are not included in the isotopic modelling. One of the Nodoushan rocks shows the highest Nd isotopic ratios, indicating the likely involvement of a more depleted mantle source.

7 Conclusions (Temporal-spatial evolution of the UDMA volcanic rock series and their implications)

495 The trace element and Sr-Nd-Pb isotopic geochemistry of the mafic volcanic rocks from the Urumieh-Dokhtar Magmatic Arc (UDMA) of Iran indicate a metasomatized mantle origin and suggest a ternary classification into LILE-rich, LILE-poor and ITE-rich series. This is interpreted to represent the nature of the metasomatizing agents involved (i.e., the fluid-rich-slab-melt, the fluid-poor-slab-melt, and more fertile segments of the mantle) in the development of the respective series. A scrutiny on the ages of the volcanic rocks of the three series compositional affinities (i.e., the LILE-rich, LILE-poor, and ITE-rich series)

500 indicates Eocene to Early Miocene ages for all three. The Neotethyan plate predating the Eocene was likely to have been narrow, about to terminate, and hot enough to furnish the partial melts that metasomatized the source mantle. The physiochemical conditions that governed slab subduction in the northern and central parts of the study area, Kahak and Ardestan respectively, were slightly different but still have significant implications. The slab subducting in the Kahak area was more hydrous, producing fluid-rich slab melts, whereas the slab subducting in the Ardestan area was thinner and of higher T,

505 producing fluid-poor slab melts. Similar Sr-Nd-Pb isotopic compositions to the other contemporary arc-type UDMA mafic volcanic rocks suggest a source modified by recycled slab (slab + sediment). Isotopic modelling indicates that the mafic volcanic UDMA rocks from the LILE-rich and LILE-poor series were derived from juvenile metasomatized mantle with mantle:slab contributions of 45:55 and 55:45 respectively where the slab melt:sediment melt involvement was 50:50 and 20:80. The ITE-rich series bear the signatures of source mantle metasomatism by slab melts prompted by and interacting with

510 asthenospheric melts in a slab window.

Supplementary data. Supplementary material contains Tables S1–S5 and Figures S1–S6.

Data availability. Data are available in EarthChem Library and can be accessed via a DOI link at https://doi.org/10.60520/IEDA/113464.

Author contribution. **MRG:** Conceptualization, Data curation, Formal analysis, Funding acquisition, Investigation,
515 Methodology, Project administration, Resources, Supervision, Validation, Visualization, Writing – original draft preparation, Writing – review & editing. **MA:** Conceptualization, Data curation, Formal analysis, Investigation, Methodology, Project administration, Resources, Software, Supervision, Validation, Visualization, Writing – original draft preparation, Writing – review & editing. **ITG:** Conceptualization, Data curation, Formal analysis, Funding acquisition, Resources, Software, Validation, Visualization, Writing – review & editing. **MB:** Conceptualization, Data curation, Formal analysis, Funding
520 acquisition, Investigation, Methodology, Resources, Software, Validation, Visualization, Writing – review & editing. **FS:** Conceptualization, Data curation, Formal analysis, Validation, Visualization, Writing – review & editing.

Competing interests. The authors declare that they have no conflict of interest.

Acknowledgments. This work is a part of the sabbatical leave that the first author spent at the University of New South Wales (UNSW, Sydney, Australia) in early 2023 as well as a part of his long-term research interest in the arc magmatism at the

525 Tarbiat Modares University (TMU, Iran). Funds and facilities provided by the UNSW, GET-OMP (Toulouse, France), and TMU are acknowledged. Valuable comments by Dr. Pier Paolo Giacomoni and Prof. Delphine Bosch are highly appreciated; these helped significantly improved the manuscript. The insightful handling of the manuscript by Prof. Massimo Coltorti is sincerely acknowledged. We would also like to thank Dr. Helen Wang and Irene Wainwright from the X-ray Fluorescence Laboratory, UNSW, Sydney for the XRF analyses and Dr. Alan Greig from the School of Geography, Earth and Atmospheric 530 Sciences, University of Melbourne, Victoria, for the ICP-MS analyses.

References

Agard, P. Omrani, J. Jolivet, L. and Mouthereau, F.: Convergence history across Zagros (Iran): Constraints from collisional and earlier deformation, Int. J. Earth Sci., 94, 401–419, doi:10.1007/s00531-005-0481-4, 2005.

Ahmadian, J. Sarjoughian, F. Lentz, D. Esna-Ashari, A. Murata, M. and Ozawa, H.: Eocene K-rich adakitic rocks in the Central 535 Iran: Implications for evaluating its Cu-Au-Mo metallogenic potential, Ore Geol. Rev., 72, 323–342, doi:10.1016/j.oregeorev.2015.07.017, 2016.

Ahmadvand, A. Ghorbani, M. R. Mokhtari, M. A. A. Chen, Y. Amidon, W. Santos, J. F. and Paydari, M.: Lithospheric mantle, asthenosphere, slab and crustal contribution to petrogenesis of Eocene to Miocene volcanic rocks from the west Alborz magmatic assemblage, SE Ahar. Iran, Geol. Mag., 158, 375–406, doi:10.1017/S0016756820000527, 2021.

540 Akbari, M., Ghorbani, M. R. Cousens, B. L. and Graham, I. T.: Quaternary post-collisional high Nb-like basalts from Bijar-Qorveh, NW Iran: a metasomatized lithospheric mantle source, Lithos, 426-427, 106781, doi:10.1016/j.lithos.2022.106781, 2022.

Akbari, M., Ghorbani, M. R. Cousens, B. L. and Graham, I. T.: A robust discrimination scheme for ocean island basalts based on Ce/Rb, Tb/La, and Ba/Nb ratios, Chem. Geol., 628, 121486, doi: 10.1016/j.chemgeo.2023.121486, 2023.

545 Alaie-Mahabadi, S. and Foudazi, M.: Geological map of the Nain quadrangle, Geological Survey of Iran, scale 1:100 000, 1 sheet, 2004.

Alavi, M.: Tectonics of the Zagros orogenic belt of Iran: New data and interpretations, Tectonophysics, 229, 211–238, doi:10.1016/0040-1951(94)90030-2, 1994.

Amidi, S. M. Nabavi, M. H. and Molla Ali, A.: Geological map of the Sarve-Bala quadrangle, Geological Survey of Iran, scale 550 1:100 000, 1 sheet, 1989.

Amini, B. and Amini Chehragh, M. R.: Geological map of the Kajan quadrangle, Geological Survey of Iran, scale 1:100 000, 1 sheet, 2003.

Atanasova, P. Marks, M. A. W. Frenzel, M. Gutzmer, J. Krause, J. and Markl, G.: Fractionation of geochemical twins (Zr/Hf, Nb/Ta and Y/Ho) and HREE-enrichment during magmatic and metamorphic processes in peralkaline nepheline syenites from 555 Norra Kärr (Sweden), Lithos, 372–373, 105667, doi:10.1016/j.lithos.2020.105667, 2020.

Babazadeh, S. Ghorbani, M. R. Bröcker, M. D'Antonio, M. Cottle, J. Gebbing, T. Mazzeo, F. C. and Ahmadi, P.: Late Oligocene-Miocene mantle upwelling and interaction inferred from mantle signatures in gabbroic to granitic rocks from the Urumieh–Dokhtar arc, south Ardestan, Iran, Int. Geol. Rev. 59, 1590–1608, doi:10.1080/00206814.2017.1286613, 2017.

Bahroudi, A. and Fonoudi, M.: Geological map of the Shahrab quadrangle, Geological Survey of Iran, scale 1:100 000, 1 sheet, 1997.

560

Benoit, M. Aguillón-Robles, A. Calmus, T. Maury, R. C. Bellon, H. Cotton, J. Bourgois, J. and Michaud, F.: Geochemical diversity of Late Miocene volcanism in southern Baja California, Mexico: Implication of mantle and crustal sources during the opening of an asthenospheric window, J. Geol. 110, 627–648, doi:10.1086/342735, 2002.

Berberian, F. and Berberian, M.: Tectono-plutonic episodes in Iran, in Delany, F. M. and Gupta, H. K. eds., Zagros, Hindu

565

Kush, Himalaya geodynamic evolution, Am. Geophys. Union, Geodynamics Series 3, 5-32, doi:10.1029/GD003p0005, 1981.

Berberian, M. and King, G. C. P.: Towards a paleogeography and tectonic evolution of Iran, Can. J. Earth Sci. 18, 210–265, doi:10.1139/e81-019, 1981.

Bouilhol, P. Jagoutz, O. Hanchar, J. M. and Dudas, F. O.: Dating the India-Eurasia collision through arc magmatic records, Earth Planet. Sci. Lett., 366, 163–175, doi:10.1016/j.epsl.2013.01.023, 2013.

570

Castillo, P. R. Rigby, S. J. and Solidum, R. U.: Origin of high field strength element enrichment in volcanic arcs: Geochemical evidence from the Sulu Arc, southern Philippines, Lithos, 97, 271–288, doi:10.1016/j.lithos.2006.12.012, 2007.

Chauvel, C. Lewin, E. Carpentier, M. Arndt, N. T. and Marini, J. C.: Role of recycled oceanic basalt and sediment in generating the Hf-Nd mantle array, Nat. Geosci., 1, 64–67, doi:10.1038/ngeo.2007.51, 2008.

Chiu, H. Y. Chung, S. L. Zarrinkoub, M. H. Mohammadi, S. S. Khatib, M. M. and Iizuka, Y.: Zircon U-Pb age constraints

575

from Iran on the magmatic evolution related to Neotethyan subduction and Zagros orogeny, Lithos, 162–163, 70–87, doi:10.1016/j.lithos.2013.01.006, 2013.

Cross, T. A. and Pilger, R. H.: Controls of subduction geometry, location of magmatic arcs, and tectonics of arc and back-arc regions, Geol. Soc. Am. Bull., 93, 545–562, doi:10.1130/0016-7606(1982)93<545:COSGLO>2.0.CO;2, 1982.

Dargahi, S. Arvin, M. Pan, Y. and Babae, A.: Petrogenesis of post-collisional A-type granitoids from the Urumieh–Dokhtar

580

magmatic assemblage, South western Kerman, Iran: Constraints on the Arabian–Eurasian continental collision, Lithos, 115, 190–204, doi:10.1016/j.lithos.2009.12.002, 2010

Defant, M. J. Jackson, T. E. Drummond, M. S. De Boer, J. Z. Bellon, H. Feigenson, M. D. Maury, R. C. and Stewart, R. H.: The geochemistry of young volcanism throughout western Panama and southeastern Costa Rica: An overview, J. Geol. Soc. London, 149, 569–579, doi:10.1144/gsjgs.149.4.0569, 1992.

585

Di Giuseppe, P. Agostini, S. Di Vincenzo, G. Manetti, P. Savaşçın, M. T. and Conticelli, S.: From subduction to strike slip‐related volcanism: insights from Sr, Nd, and Pb isotopes and geochronology of lavas from Sivas-Malatya region, Central Eastern Anatolia, Int. J. Earth Sci., 110, 849–874, doi:10.1007/s00531-021-01995-0, 2021.

Dong, K. Chen, S. Graham, I. Zhao, J. Fu, P. Xu, Y. Tian, G. Qin, W. and Chen, J.: Geochemical behavior during mineralization and alteration events in the Baiyinchang volcanic-hosted massive sulfide deposits, Gansu Province, China, Ore Geol. Rev., 91,

590

559–572, doi:10.1016/j.oregeorev.2017.09.002, 2017.

Emami, M. H. Sadeghi, M. M. M. and Omrani, S.J.: Magmatic map of Iran. Tehran, Geological Survey of Iran, 1993.

Ewart, A. Collerson, K. D. Regelous, M. Wendt, J. I. and Niu, Y.: Geochemical evolution within the Tonga-Kermadec-Lau arc-back-arc systems: the role of varying mantle wedge composition in space and time, J. Petrol. 39, 331–368, doi.org/10.1093/petroj/39.3.331, 1998.

595   Farner, M. J. and Lee, C. A.: Effects of crustal thickness on magmatic differentiation in subduction zone volcanism: A global study, Earth Planet. Sci. Lett., 470, 96–107, doi:10.1016/j.epsl.2017.04.025, 2017.

Ghalamghash, J. Babakhani, A.R. Bahroudi, A. and Fonoudi, M.: Geological map of the Kahak quadrangle, Geological Survey of Iran, scale 1:100 000, 1 sheet, 1988.

Ghalamghash, J. Mohammadiha, K. and Ghahraie Pour M.: Geological map of the Kafeh-Taghestan quadrangle, Geological

600   Survey of Iran, scale 1:100 000, 1 sheet, 2005.

Ghorbani, M. R. and Middlemost, E. A. K.: Geochemistry of pyroxene inclusions from the Warrumbungle Volcano, New South Wales, Australia, Am. Min., 85, 1349–1367, doi:10.2138/am-2000-1003, 2000.

Ghorbani, M. R.: Lead enrichment in Neotethyan volcanic rocks from Iran: The implications of a descending slab, Geochem. J., 40, 557–568. doi:10.2343/geochemj.40.557, 2006.

605   Ghorbani, M. R. and Bezenjani, R. N.: Slab partial melts from the metasomatizing agent to adakite, Tafresh Eocene volcanic rocks, Iran, Isl. Arc, 20, 188–202, doi:10.1111/j.1440-1738.2010.00757.x, 2011.

Ghorbani, M. R. Graham, I. T. and Ghaderi, M.: Oligocene-Miocene geodynamic evolution of the central part of Urumieh-Dokhtar arc of Iran, Int. Geol. Rev., 56, 1039–1050, doi:10.1080/00206814.2014.919615, 2014.

Gill, J. B.: Orogenic Andesites and Plate Tectonics. Springer-Verlag, New York, doi:10.1007/978-3-642-68012-0, 1981.

610   Hart, S. R.: A large-scale isotope anomaly in the Southern Hemisphere mantle, Nat., 309, 753–757, doi:10.1038/309753a0, 1984.

Hastie, A. R. Mitchell, S. F. Kerr, A. C. Minifie, M. J. and Millar, I. L.: Geochemistry of rare high-Nb basalt lavas: are they derived from a mantle wedge metasomatised by slab melts?, Geochim. Cosmochim. Acta., 75, 5049.72, doi:10.1016/j.gca.2011.06.018, 2011.

615   Hauff, F. Hoernle, K. and Schmidt, A.: Sr–Nd–Pb composition of Mesozoic Pacific oceanic crust (Site 1149 and 801, ODP Leg 185): Implications for alteration of ocean crust and the input into the Izu–Bonin–Mariana subduction system, Geochem. Geophys. Geosyst., 4, doi:10.1029/2002GC000421, 2003.

Hawkesworth, C. Turner, S. Peate, D. McDermott, F. and Calsteren, P. V.: Elemental U and Th variations in island arc rocks: implications for U-series isotopes, Chem. Geol., 139, 207-221, doi:10.1016/S0009-2541(97)00036-3, 1997.

620   Hermann, J. and Spandler, C.J.: Sediment Melts at Sub-arc Depths: an Experimental Study, J. Petrol 49, 717–740, doi: 10.1093/petrology/egm073, 2008.

Hildreth, W. and Moorbath, S.: Crustal contributions to arc magmatism in the Andes of central Chile, Contrib. Mineral. Petrol., 98, 455–489, doi:10.1007/BF00372365, 1988.

625 Horton, B. K. Hassanzadeh, J. Stockli, D. F. Axen, G. J. Gillis, R. J. Guest, B. Amini, A. Fakhari, M. D. Zamanzade, S. M. and Grove, M.: Detrital zircon provenance of Neoproterozoic to Cenozoic deposits in Iran: Implications for chronostratigraphy and collisional tectonics, Tectonophysics, 451, 97–122, doi:10.1016/j.tecto.2007.11.063, 2008

Jicha, B. R. and Singer, B. S.: Volcanic history and magmatic evolution of Seguam Island, Aleutian Island arc, Alaska, Geol. Soc. Am. Bull., 118, 805-822, doi:10.1130/B25861.1, 2006.

Jolani Varzeghani, A.: Trace elements and isotope geochemistry of Nodoushan volcanic rocks, M.Sc. Thesis, Tarbiat Modares
630 University, Tehran, Iran, 2017.

Kelemen, P. B. Hanghøj, K. and Greene, A. R. One view of the geochemistry of subduction-related magmatic arcs, with an emphasis on primitive andesite and lower crust, Rudnick, R. L. (ed.) Treatise Geochem., 3. The Crust, Elsevier, Amsterdam, 593–659, doi:10.1016/B0-08-043751-6/03035-8, 2005.

Kepezhinskas, P. K. Defant, M. J. and Drummond, M. S.: Na metasomatism in the island-arc mantle by slab melt-peridotite
635 interaction: evidence from mantle xenoliths in the North Kamchatka arc, J. Petrol., 36, 1505–1527, doi: 10.1093/oxfordjournals.petrology.a037263, 1995.

Kepezhinskas, P. McDermott, F. Defant, M. J. Hochstaedter, A., Drummond, M. S. Hawkesworth, C. J. Kokoskov, A. Maury, R. and Bellon, H.: Trace element and Sr–Nd–Pb isotopic constraints on a three-component model of Kamchatka Arc petrogenesis, Geochim. Cosmochim. Acta, 61, 577–600, doi:10.1016/S0016-7037(96)00349-3, 1997.

640 Khalatbari Jafari, M. and Alaie-Mahabadi, S.: Geological map of the Natanz quadrangle, Geological Survey of Iran, scale 1:100 000, 1 sheet, 1995.

Khodami, M.: Pb isotope geochemistry of the late Miocene–Pliocene volcanic rocks from Todeshk, the central part of the Urumieh–Dokhtar magmatic arc, Iran: Evidence of an enriched mantle source, J. Earth Syst. Sci., 128, doi:10.1007/s12040-019-1185-7, 2019.

645 Kress, V. C. and Carmichael, I. S. E.: The compressibility of silicate liquids containing Fe_2O_3 and the effect of composition, temperature, oxygen fugacity and pressure on their redox states, Contrib. Mineral. Petrol., 108, 82–92, doi:10.1007/BF00307328, 1991.

Li, C. F. Li, X. H. Li, Q. L. Guo, J. H. and Li, X. H.: Directly determining $^{143}Nd/^{144}Nd$ isotope ratios using thermal ionization mass spectrometry for geological samples without separation of Sm-Nd, J. Anal. At. Spectrom., 26, doi:10.1039/C0JA00081G,
650 2011.

Li, C. F. Li, X. H. Li Q. L. Guo, J. H. Li, X. H. and Yang, Y. H.: Rapid and precise determination of Sr and Nd isotopic ratios in geological samples from the same filament loading by thermal ionization mass spectrometry employing a single-step separation scheme, Anal. Chim. Acta, 727, 54–60, doi:10.1016/j.aca.2012.03.040, 2012.

Linnen, R. L. and Keppler, H.: Melt composition control of Zr/Hf fractionation in magmatic processes, Geochim. Cosmochim.
655 Acta, 66, 3293–3301, doi:10.1016/S0016-7037(02)00924-9, 2002.

Manea, V. C. Leeman, W. P. Gerya, T. Manea, M. and Zhu, G.: Subduction of fracture zones controls mantle melting and geochemical signature above slabs, Nat. Commun., 5, 5095, doi:10.1038/ncomms6095, 2014.

Mayborn, K. R. and Lesher, C. E.: MagPath: An Excel-based Visual Basic program for forward modeling of mafic magma crystallization, Comput. and Geosci., 3, 1900–1903, doi: 10.1016/j.cageo.2011.02.017, 2011.

660 Mohajjel, M. and Fergusson, C. L.: Dextral transpression in Late Cretaceous continental collision, Sanandaj-Sirjan Zone, western Iran, J. Struct. Geol., 22, 1125–1139, doi:10.1016/S0191-8141(00)00023-7, 2000.

Moinevaziri, H.: Volcanisme Tertiaire et Quaternaire en Iran, Paris-Sud Orsay, These d Etat, 1985.

Moradi, S. Ghorbani, M. R. Jiang, S. Y. and Christiansen, E. H.: Mafic to intermediate composition intrusions from the Kahak area, central Urumieh-Dokhtar arc of Iran: transition from Eocene to Miocene intra-arc extensional magmatism, Mineral.

665 Petrol., 115, 445–466, doi:10.1007/s00710-021-00745-z, 2021.

Morishita, T. Arai, S. and Tamura, A.: Petrology of an apatite-rich layer in the Finero phlogopite–peridotite, Italian Western Alps; implications for evolution of a metasomatising agent, Lithos, 69, 37–49, doi:10.1016/S0024-4937(03)00046-X, 2003.

Norrish, K. and Hutton, J. T.: An accurate X-ray spectrographic method for the analysis of a wide range of geological samples, Geochim. Cosmochim. Acta, 33, 431–453, doi:10.1016/0016-7037(69)90126-4, 1969.

670 Omrani, J. Agard, P. Whitechurch, H. Benoit, M. Prouteau, G. and Jolivet, L.: Arc-magmatism and subduction history beneath the Zagros Mountains, Iran: A new report of adakites and geodynamic consequences, Lithos, 106, 380–398, doi:10.1016/j.lithos.2008.09.008, 2008.

O'Reilly, S. Y. Griffin, W. L. and Ryan, C. G.: Residence of trace elements in metasomatised spinel lherzolite xenoliths: A proton-microprobe study, Contrib. Mineral. Petrol., 109, 98–113, doi: 10.1007/BF00687203, 1991.

675 Pearce, J. A.: Trace element characteristics of lavas from destructive plate boundaries, Thorpe, R. S. ed. Orogenic andesites and related rocks, Chichester, England: John Wiley and Sons, 528–548, 1982.

Pearce, J. A. Bender, J. F. Delong, S. E. Kidd, W. S. F. Low, P. J. Guner, Y. Sargolu, F. Yilmaz, Y. Moorbath, S. and Mitchell, J. G.: Genesis of collision volcanism in eastern Anatolia, Turkey, J. Volcanol. Geotherm. Res., 44, 189–229, doi:10.1016/0377-0273(90)90018-B, 1990.

680 Pickering-Witter, J. M. and Johnston, A. D.: The effects of variable bulk composition on the melting systematics of fertile peridotitic assemblages, Contrib. Mineral. Petrol., 140, 190–211, doi:10.1007/s004100000183, 2000.

Pin, C. and Gannoun, A.: Integrated Extraction Chromatographic Separation of the Lithophile Elements Involved in Long-Lived Radiogenic Isotope Systems (Rb–Sr, U–Th–Pb, Sm–Nd, La–Ce, and Lu–Hf) Useful in Geochemical and Environmental Sciences, Anal. Chem., 89, 2411–2417, doi:10.1021/acs.analchem.6b04289, 2017.

685 Plank, T. and Langmuir, C. H.: An evaluation of the global variations in the major element chemistry of arc basalts, Earth Planet. Sci. Lett., 90, 349–370, doi:10.1016/0012-821X(88)90135-5, 1988.

Powell, R.: Inversion of the assimilation and fractional crystallization (AFC) equations; characterization of contaminants from isotope and trace element relationships in volcanic suites, J. Geol. Soc., 141, 447–452, doi:10.1144/gsjgs.141.3.0447, 1984.

690 Prelević, D. Foley, S. F. Romer, R. and Sonticelli, S.: Mediterranean Tertiary lamproites derived from multiple source components in postcollisional geodynamics, Geochim. Cosmochim. Acta, 72, 2125–2156, doi:10.1016/j.gca.2008.01.029, 2008.

Rabiee, A. Rossetti, F. Asahara, Y. Azizi, H. Lucci, F. Lustrino, M. and Nozaem, R.: Long-lived, Eocene-Miocene stationary magmatism in NW Iran along a transform plate boundary, Gondwana Res., 85, 237–262, doi: 10.1016/j.gr.2020.03.014, 2020.

695 Radfar, J. and Alaie-Mahabadi, S.: Geological map of the Kashan quadrangle, Geological Survey of Iran, scale 1:100 000, 1 sheet, 1993.

Radfar, J. and Amini Chehragh, M. R.: Geological map of the Ardestan quadrangle, Geological Survey of Iran, scale 1:100 000, 1 sheet, 1999.

Radfar, J. Kohansal, R. and Zolfaghari, S.: Geological map of the Kuhpayeh quadrangle, Geological Survey of Iran, scale 700 1:100 000, 1 sheet, 2002.

Reagan, M. K. and Gill, J. B.: Coexisting calcalkaline and high-niobium basalts from Turrialba volcano, Costa Rica: implications for residual titanites in arc magma sources, J. Geophys. Res., 94, 4619–4633, doi:10.1029/JB094iB04p04619, 1989.

Schiano, P. Clocchiatti, R. Shimizu, N. Maury, R. C. Jochum, K. P. and Hofmann, A. W.: Hydrous, silica-rich melts in the 705 sub-arc mantle and their relationship with erupted arc lavas, Nat., 377, 595–600, doi:10.1038/377595a0, 1995.

Sepidbar, F. Shafaii Moghadam, H. Zhang, L. Li, J. W. Ma, J. Stern, R. J. and Lin, C.: Across–arc geochemical variations in the Paleogene magmatic belt of Iran, Lithos, 344–345, 280–396, doi:10.1016/j.lithos.2019.06.022, 2019.

Sepidbar, F. Karsli, O. Palin, R. M. and Casetta, F.: Cenozoic temporal variation of crustal thickness in the Urumieh-Dokhtar and Alborz magmatic belts, Iran, Lithos, 400–401, 106401, doi:10.1016/j.lithos.2021.106401, 2021.

710 Shafaii Moghadam, H. Ghorbani, G. Zaki Khedr, M. Fazlnia, N. Chiaradia, M. Eyuboglu, Y. Santosh, M. Francisco, C. G. Martinez, M, L. Gourgaud, A. and Arai, S: Late Miocene K-rich volcanism in the Eslamieh Peninsula (Saray), NW Iran: Implications for geodynamic evolution of the Turkish–Iranian High Plateau, Gondwana Res., 26, 1028–1050, doi:10.1016/j.gr.2013.09.015, 2014.

Shahabpour, J.: Island-arc affinity of the central Iranian volcanic belt, J. Asian Earth Sci., 30, 652–665, 715 doi:10.1016/j.jseaes.2007.02.004, 2007.

Spikings, R. Cochrane, R. Villagomez, D. Van der Lelij, R. Vallejo, C. Winkler, W. and Beate, B.: The Geological History of Northwestern South America: from Pangaea to the Early Collision of the Caribbean Large Igneous Province (290-75 Ma), Gondwana Res., 27, 95–139, doi:10.1016/j.gr.2014.06.004, 2015.

Stracke, A. Bizimis, M. and Salters, V. J. M.: Recycling oceanic crust: quantitative constraints, Geochem. Geophys. Geosyst., 720 4, 8003, doi:10.1029/2001GC000223, 2003.

Stracke, A. Hofmann, A.W. and Hart, S.R..: FOZO, HIMU, and the rest of the mantle zoo. Geochem. Geophys. Geosyst. 6, Q05007, doi:10.1029/2004GC000824, 2005.

Straub, S. M. Gómez-Tuena, A. Bindeman, I. N. Bolge, L. L. Brandle, P. A. Espinasa-Perena, R. Solari, L. Stuart, F. M. Vannucchi, P. and Zellmer, G. F.: Crustal recycling by subduction erosion in the central Mexican Volcanic Belt, Geochim.

725   Cosmochim. Acta, 166, 29–52, doi:10.1016/j.gca.2015.06.001, 2015.

Streck, M. J. Leeman, W. P. and Chesley, J.: High-magnesian andesite from Mount Shasta: a product of magma mixing and contamination, not a primitive mantle melt, Geology, 35, 351–354, doi:10.1130/G23286A.1, 2007.

Sun, S.S. and McDonough, W.F.: Chemical and isotopic systematics of oceanic basalts: Implications for mantle composition and processes. In: Saunders, A. D. and Norry, M. J. (Eds.), Magmatism in the Ocean Basins, J. Geol. Soc., London, Special

730   Publications, 42, 313–345, doi:10.1144/gsl.sp.1989.042.01.19, 1989.

Szabó, C. Falus, G. Zajacz, Z. Kovács, I. and Bail, E.: Composition and evolution of lithosphere beneath the Carpathian-Pannonian Region: a review, Tectonophysics 393, 119–137, doi.org/10.1016/j.tecto.2004.07.031, 2004.

van Hinsbergen, D. J. J. Torsvik, T. H. Schmid, S. M. Maţenco, L. C. Maffione, M. Vossers, R. L. M. Gürer, D. and Spakman, W.: Orogenic architecture of the Mediterranean region and kinematic reconstruction of its tectonic evolution since the Triassic,

735   Gondwana Res., 81, 79–229, doi:10.1016/j.gr.2019.07.009, 2020.

Verdel, C. Wernicke, B. P. Hassanzadeh, J. and Guest, B.: A Paleogene extensional arc flare up in Iran. Tectonics 30, 1–20, doi:10.1029/2010TC002809, 2011.

Whitney, D. L. and Evans, B. W.: Abbreviations for names of rock-forming minerals, American Mineralogist, 95, 185–187, doi:10.2138/am.2010.3371, 2010.

740   Wilson, B. M.: Igneous Petrogenesis: A Global Tectonic Approach, Chapman and Hall, London, doi:10.1007/978-1-4020-6788-4, 1989.

Xia, L. Q.: The geochemical criteria to distinguish continental basalts from arc related ones, Earth Sci. Rev., 139, 195–212, doi:10.1016/j.earscirev.2014.09.006, 2014.

Yeganehfar, H. Ghorbani, M. R. Shinjo, R. and Ghaderi, M.: Magmatic and geodynamic evolution of Urumieh-Dokhtar basic

745   volcanism, Central Iran: major, trace element, isotopic, and geochronologic implications, Int. Geol. Rev., 55, 767–786, doi:10.1080/00206814.2012.752554, 2013.

Zahedi, M. and Rahmati, M.: Geological map of the Tarq quadrangle, Geological Survey of Iran, scale 1:100 000, 1 sheet, 2002.

Zheng, Y. F.: Subduction zone geochemistry, Geosci. Front., 10, 1223–1254, doi:10.1016/j.gsf.2019.02.003, 2019.

750